Decoupling a Cooper-Pair Box to Enhance the Lifetime to 0.2 ms

Z. Kim,[1,2] B. Suri,[1,2] V. Zaretskey,[1,2] S. Novikov,[1,2] K. D. Osborn,[1] A. Mizel,[1] F. C. Wellstood,[2,3] and B. S. Palmer[1]

[1]*Laboratory for Physical Sciences, College Park, Maryland 20740, USA*

[2]*Department of Physics, University of Maryland, College Park, Maryland 20742, USA*

[3]*Joint Quantum Institute and Center for Nanophysics and Advanced Materials, College Park, Maryland 20742, USA*

(Received 21 September 2010; published 22 March 2011)

We present results on a circuit QED experiment in which a separate transmission line is used to address a quasilumped element superconducting microwave resonator which is in turn coupled to an $Al/AlO_x/Al$ Cooper-pair box charge qubit. With our device, we find a strong correlation between the lifetime of the qubit and the inverse of the coupling between the qubit and the transmission line. At the smallest coupling we measured, the lifetime of the Cooper-pair box was $T_1 = 200\ \mu s$, which represents more than a twentyfold improvement in the lifetime of the Cooper-pair box compared with previous results. These results imply that the loss tangent in the AlO_x junction barrier must be less than about 4×10^{-8} at 4.5 GHz, about 4 orders of magnitude less than reported in larger area $Al/AlO_x/Al$ tunnel junctions.

DOI: 10.1103/PhysRevLett.106.120501 PACS numbers: 03.67.Lx, 42.50.Pq, 84.40.Dc, 85.25.Cp

The use of high quality factor superconducting resonators has many applications in solid-state and atomic physics including microwave kinetic inductance detectors [1] and in the quantum information sciences in the form of circuit quantum electrodynamics [2–4]. Understanding and minimizing the sources of energy loss in these systems has a general technological importance for all of these topics to improve the sensitivities of microwave kinetic inductance detectors and coherence times for qubits. For superconducting qubits, energy loss has been attributed to various mechanisms, including discrete charge two-level fluctuators coupled to the qubit [5,6], dielectric loss [7], nonequilibrium quasiparticles [8], and lossy higher order electromagnetic modes of the electromagnetic field which are coupled to the qubit [9].

Here, we report the observation of relaxation times in a Cooper-pair box (CPB) that are 1 order of magnitude larger than previously reported. Our design builds on the circuit quantum electrodynamics approach [2,10,11]: We coupled the CPB to a resonator and used perturbations of the resonator frequency to read out the state of the CPB over one octave in frequency. In contrast to previous work, however, we used a lumped element design for the resonator and addressed it by using a separate transmission line. In our experiment, we find that a key reason for obtaining the long lifetimes was decoupling the CPB from the transmission line.

Our CPB consists of a small (100 nm $\times$ 2 μm $\times$ 30 nm thick) superconducting Al island connected to superconducting leads by two ultrasmall Josephson junctions [see Fig. 1(c)]. By applying a dc voltage V_g that is capacitively coupled to the island with capacitance C_g^*, we can change the system's electrostatic charging energy, and by varying the magnetic flux through the superconducting loop, we can modulate the critical current I_0 and therefore the Josephson energy $E_J = \hbar I_0/2e$. Restricting consideration to the two lowest levels, the Hamiltonian of the CPB can be written as

$$H_{\mathrm{CPB}} = \frac{\hbar\omega_a}{2}\sigma_z, \tag{1}$$

where $\hbar\omega_a = \sqrt{[4E_c(1-n_g)]^2 + E_J^2}$, $E_c = e^2/2C_\Sigma$ is the electrostatic charging energy constant, $n_g = C_g^* V_g/e$ is the reduced gate voltage, and σ_z is a Pauli spin matrix.

We coupled our CPB to a quasilumped element resonator [Fig. 1(a)] and measured the CPB at the charge degeneracy point while it was tuned over one octave in frequency. When the CPB is coupled to a resonator and the detuning between the qubit and the resonator ($\Delta = \omega_a - \omega_r$) is large compared to the strength of the coupling g between them, the Hamiltonian for the combined system is approximately

$$H \cong \hbar\left(\omega_r + \frac{g^2}{\Delta}\sigma_z\right)\left(a^\dagger a + \frac{1}{2}\right) + \frac{\hbar\omega_a}{2}\sigma_z, \tag{2}$$

where $\hbar g = (eC_g/C_\Sigma)\sqrt{\hbar\omega_r/2C}$, C is the capacitance of the resonator with resonance frequency ω_r, and C_g is the capacitance between the resonator and the island of the CPB [10,11]. Depending on the state of the qubit, Eq. (2) predicts that the bare resonance frequency ω_r is shifted by $\pm g^2/\Delta$. For $g/2\pi = 5$ MHz and $\Delta/2\pi = 1$ GHz, we find that the maximum dispersive frequency shift of the resonator's resonance frequency is $g^2/2\pi\Delta = 25$ kHz.

To measure these small frequency shifts we have designed and fabricated, using photolithographic lift-off techniques, a high-Q superconducting resonator made from a 100 nm thick film of Al on a c-plane sapphire wafer. The resonator consists of a coplanar meander-line inductor (~ 2 nH) and an interdigital capacitor (~ 400 fF) coupled to a transmission line [see Fig. 1(a)]. The resonance frequency of our resonator was $\omega_r/2\pi = 5.44$ GHz,

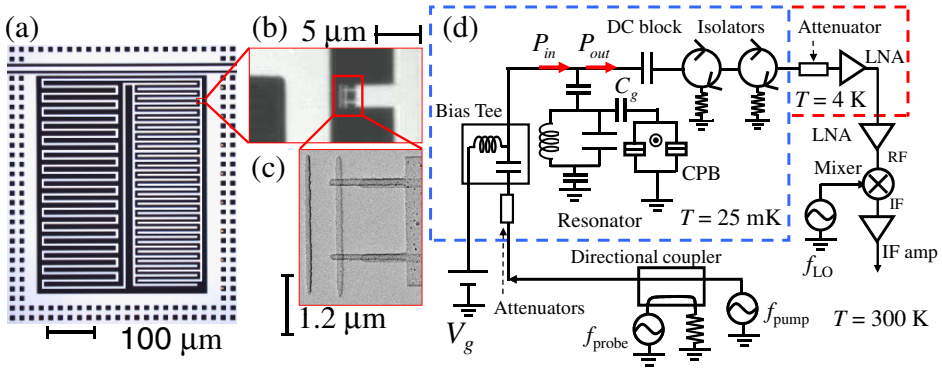

FIG. 1 (color online). (a) Optical image of a quasilumped element resonator coupled to a transmission line and surrounded by a ground plane. White regimes are aluminum, and black regimes are sapphire. (b) Optical image of the CPB close to the interdigital capacitor. (c) Scanning electron micrograph of the CPB. (d) Schematic of the measurement setup. Two microwave tones are sent to the device on the mixing chamber through microwave lines and attenuators at different temperatures. On the mixing chamber the microwave tones are combined with a dc voltage before the device. After the device the signal passes through two isolators, is amplified at both 4 and 300 K, mixed to a smaller intermediate frequency, and then digitized on an oscilloscope.

the loaded quality factor was $Q_L = 22\,000$, and the internal quality factor was $Q_i = 32\,000$. Subsequently, the CPB was fabricated by using e-beam lithography and double-angle evaporation (with an oxidation in between the two evaporations) to form the small Josephson junctions [12]. We used a bilayer of MMA(8.5)MMA copolymer (mixture of polymethyl methacrylate and 8.5% methacrylic acid) and ZEP520A (methylstyrene/chloromethyl acrylate copolymer) as the electron beam resist and the 30 nm thick Al island and 50 nm thick Al leads were deposited in an electron beam evaporator [see Figs. 1(b) and 1(c)].

The device was packaged in an rf-tight Cu box and bolted to the mixing chamber of an Oxford Instruments Kelvinox 100 dilution refrigerator. To reduce Johnson-Nyquist noise from higher temperatures, we used cold attenuators on the input microwave line and two isolators on the output line [see Fig. 1(d)]. The input microwave power had 10 dB of attenuation at 4 K, 20 dB at 0.7 K, and 30 dB on the mixing chamber at 25 mK. On the output line, both isolators on the mixing chamber had a minimum isolation of 18 dB between 4 and 8 GHz. The output microwave signal was amplified with a high-electron-mobility transistor amplifier sitting in the He bath. To allow a dc gate voltage bias to be applied to the island of the CPB from the transmission line, a bias tee was placed on the transmission line before the device and a dc block was placed on the transmission line after the device [see Fig. 1(d)].

Figure 2(a) shows a plot of the transition spectrum of the CPB qubit. This spectrum was taken by measuring the phase of the transmitted microwaves at the resonator's bare resonance frequency ($f_r = 5.44$ GHz) while sweeping the dc gate voltage and stepping the frequency of a second microwave source from 6.2 to 8.4 GHz. When the second microwave source is resonant with the transition between the two lowest states of the CPB, the CPB is excited. This causes a change in ω_r [see Eq. (2)] and a change in the phase of the transmitted signal. For these measurements the average number of photons in the resonator was $\bar{n} = 20$ photons. From fitting this spectrum, we extract $E_c/h = 6.24$ GHz and $E_J/h = 6.35$ GHz. Using these parameters and the measured dispersive shift ($g^2/2\pi\Delta \simeq 27$ kHz), we extracted the coupling between the resonator and the CPB: $g/2\pi = 5$ MHz.

To measure Rabi oscillations, we applied magnetic flux to set $E_J/h = 6.15$ GHz, dc biased the gate voltage at the charge degeneracy point $n_g = 1$, and delivered a short pulse of microwaves at $f = 6.15$ GHz while continuously monitoring the phase of the resonator with an average of $\bar{n} = 20$ photons. Figure 2(b) shows a false color plot of the measured phase (which has been calibrated in terms of the probability of occupancy of the excited state) as a function of time after sending the pulse and as a function of the length of the pulse. Figure 2(c) presents a line cut through 2(b); we see clear driven oscillations of the state of the qubit.

Figure 2(d) shows a plot of the probability P_e of occupying the excited state as a function of time after sending a π pulse to the qubit at $f = 6.15$ GHz and $n_g = 1$. For $P_e > 5\%$, the relaxation is well fit by an exponential with a decay time of $T_1 = 30$ μs. We also varied the Josephson energy from a maximum of $E_J/h = 19$ GHz and measured T_1 at the charge degeneracy point over one octave in the CPB transition frequency, from 3.8 to 8.5 GHz [black squares in Fig. 3(b)]. While $T_1 \sim 30$ μs for frequencies above f_r, we discover that the CPB attains a striking lifetime of $T_1 = 200$ μs below f_r at $f = 4.5$ GHz.

Some of the qualitative features in Fig. 3(b) can be understood. In particular, the depressions in T_1 at $f = 4.18$ GHz and $f = 5.67$ GHz correlate to changes in the measured transmission of microwaves through the transmission line [see Fig. 3(a)] and are likely due to the packaging of our device ($f = 4.18$ GHz) or imperfections in a microwave component ($f = 5.67$ GHz). Also, the dip near

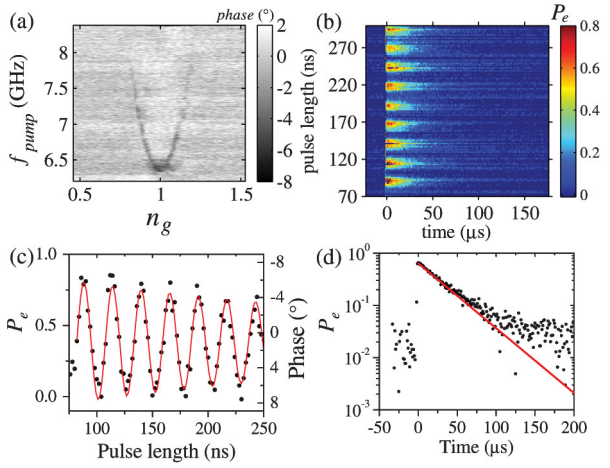

FIG. 2 (color). (a) Measured spectrum of the CPB. The gray-scale plot shows the change in phase of the transmitted microwaves at the probe frequency as a function of the pump frequency and n_g. (b) Rabi oscillation of the CPB qubit for microwave drive at $f = 6.15$ GHz. (c) Line cut of (b) along the pulse length at a measurement time of 2 μs. The maximum measured population in the excited state was about 80%. From the fit (red curve), the extracted Rabi frequency was 39 MHz. (d) Energy relaxation measurement of the CPB from the excited state. The red line shows a fit with $T_1 \simeq 30$ μs.

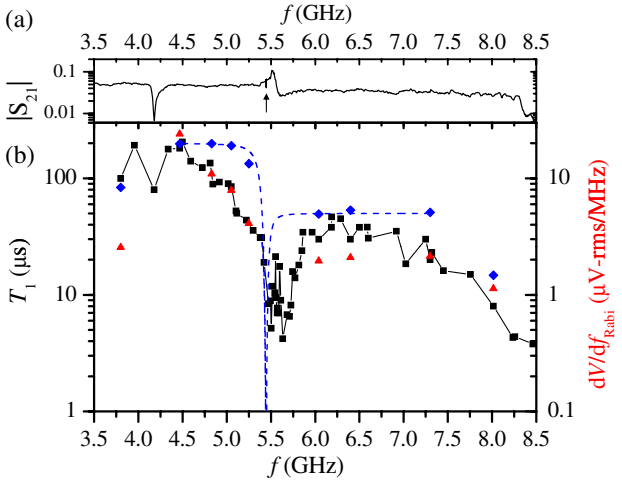

FIG. 3 (color online). (a) Plot of the ratio of the transmitted output voltage before the mixer in Fig. 1 to input voltage (S_{21}) versus frequency through the system. The arrow at 5.44 GHz identifies the resonance of the resonator. (b) Log plot of measured T_1 versus frequency (filled squares) and model for T_1 (filled diamonds) based on the measured coupling to quantum noise from 50 Ω. The dashed blue curve shows the contribution to loss from coupling to the resonator plus an additional decay rate of $T_1^{-1} = 5 \times 10^3$ s^{-1} below f_r and $T_1^{-1} = 2 \times 10^4$ s^{-1} above f_r. Right axis: Inverse of the measured coupling (Rabi frequency divided by applied rms voltage) between the transmission line and the CPB versus f (red filled triangles).

$f_r = 5.44$ GHz is consistent with enhanced spontaneous emission at the resonator frequency due to the Purcell effect [see the dashed blue curve in Fig. 3(b)] [9].

Next, we studied the coupling between the qubit and the microwave drive to understand the steady change in T_1 below f_r. At several values of f, we measured the change in the frequency f_{Rabi} of the Rabi oscillations with microwave drive voltage V. The red triangles in Fig. 3(b) show dV/df_{Rabi} versus f. This quantity indicates how decoupled the transmission line is from the qubit; when dV/df_{Rabi} is large, the qubit responds only weakly to a change in V, and when dV/df_{Rabi} is small, the qubit responds strongly to a change in V. While the simple model for our system [Fig. 1(d)] does not predict this behavior of the coupling, we note that the coupling is changing near and between additional resonances in the system which can produce a nontrivial dependence of dV/df_{Rabi} on f. We find that we can achieve good agreement between the experimental dV/df_{Rabi} and a theoretical calculation that augments the simple circuit of Fig. 1(d) with an additional LC circuit which is coupled to the transmission line and the qubit to model the microwave packaging resonance at $f = 4.18$ GHz.

A close relationship between T_1 and the decoupling dV/df_{Rabi} is evident in the figure. If we assume that the qubit is capacitively coupled to a $Z_0 = 50$ Ω quantum dissipative environment at the input and output microwave lines, then the decay rate is given by [13]

$$T_1^{-1} = \left(\frac{df_{\mathrm{Rabi}}}{dV}\right)^2 8\pi^2 Z_0 h f. \tag{3}$$

The filled diamonds in Fig. 3(b) show that Eq. (3) with an additional unknown fixed decay rate of $T_1^{-1} = 5 \times 10^3$ s^{-1} is in reasonably good qualitative agreement with the data (filled squares). This relationship suggests that decoupling the qubit from the noisy transmission line in our experiment was essential to allowing T_1 to reach 30 μs at most values of f and to attain 200 μs at $f = 4.5$ GHz.

The measured lifetime also places a bound on charge noise in the CPB. If charge noise is the dominant mechanism producing relaxation, then the spectral density of charge noise S_Q at positive frequencies is related to T_1 at the charge degeneracy point by [13–15]

$$S_Q(+f) = \left(\frac{e\hbar}{2E_c}\right)^2 \frac{1}{T_1}. \tag{4}$$

Using Eq. (4) and the measured value of T_1 at 4.5 GHz, we get an upper bound on the spectral density of charge noise of $S_Q(f = 4.5\ \mathrm{GHz}) \leq 10^{-18}\ e^2/\mathrm{Hz}$. This level of charge noise is approximately an order of magnitude smaller than the bound measured by Vion *et al.* [16]. If we assume that S_Q has a $1/f$ dependence, then the symmetrized *classical* spectral density of charge noise at 1 Hz would be approximately $S_Q(f = 1\ \mathrm{Hz}) = 2(10^{-4})^2\ e^2/\mathrm{Hz}$, a value that is 2 orders of magnitude smaller than is typically measured at low frequencies [17,18] and similar to the best values reported in stacked single electron transistors [19].

Our T_1 measurements also place a bound on dielectric loss in the Josephson junctions. If T_1 is limited by dissipation in the junction, then the effective resistance of the tunnel junctions is related to the charge noise S_Q by

$$R = \frac{2\hbar}{\omega S_Q} = \frac{T_1}{C_\Sigma}\left(\frac{4E_c}{E_J}\right). \quad (5)$$

At $E_J/h = 4.5$ GHz, where $T_1 = 200$ μs, this yields $R \sim 3 \times 10^{11}$ Ω. If this dissipation were due to dielectric loss in the amorphous AlO_x tunnel junction barrier, then one would find $\tan\delta = (R\omega C_\Sigma)^{-1} = 4 \times 10^{-8}$, which appears to be 4 orders of magnitude smaller than most amorphous dielectrics at both low temperatures and low microwave powers [7]. A possible explanation is that the loss is due to a few discrete two-level fluctuators in the ultrasmall junctions. Spectroscopic measurements on CPB devices have shown anomalous avoided level crossings with splitting sizes on the order of 50 MHz and decay rates due to the two-level fluctuator on the order of 10 μs^{-1} [6]. If we take these parameters and assume that the two-level fluctuator resonance is detuned by 2 GHz from the CPB resonance, then the T_1 from a single fluctuator would be approximately 160 μs.

Another metric of charge noise can be found from dephasing measurements. To minimize dephasing from photons in the resonator [10], the power at f_r was pulsed on only after the state of the CPB was manipulated. At $E_J/h = 6.4$ GHz we find a Ramsey decay time of $T_2^* = 70$ ns. Assuming $1/f$ charge noise is the dominant free induction dephasing mechanism [14], then at $n_g = 1$ the standard deviation of the charge noise (σ_Q) obeys [14]

$$\sigma_Q^2 = \frac{1}{T_2^*}\frac{E_J}{(4E_c)^2}\frac{2e^2\hbar}{\eta}, \quad (6)$$

where $\eta = \ln(f_{\max}/f_{\min})$ and $f_{\min}$ and $f_{\max}$ are the minimum and maximum bandwidth of the measurement, respectively. Using Eq. (6) we find $\sigma_Q = (2 \times 10^{-3}e)^2$, which is a fairly typical value for the amplitude of $1/f$ charge noise [17,18]. Measurements of the decay of Rabi oscillations showed a maximum decay time of $T' \simeq 1$ μs.

We also obtained some measurements on a second device with a charging energy of $E_c/h = 12.48$ GHz. The lifetime of that device at $f = E_J/h = 7.5$ GHz was $T_1 = 8$ μs, which from Eq. (4) gives $S_Q(f = 7.5\ \text{GHz}) = 5 \times 10^{-18}\ e^2/\text{Hz}$. This value is within a factor of 2 of the device discussed in this Letter at $f = 7.5$ GHz. Unfortunately, we did not obtain T_1 measurements on this second device over a wide range of frequency before the device stopped functioning.

In conclusion, we have measured the spectrum, excited state lifetime, and Rabi oscillations of a CPB qubit over one octave in transition frequency. We find T_1 varies from 4 μs at $f = 8$ GHz up to 200 μs at $f = 4.5$ GHz. The longest lifetime places an upper bound on the spectral density of charge noise which is $S_Q(f = 4.5\ \text{GHz}) \leq 10^{-18}\ e^2/\text{Hz}$ at 4.5 GHz. Our measurements place a remarkably small upper bound on dielectric loss in the junction barrier. While the exact source of improvement in the lifetime of our CPB compared with other results [11,14,16] is unknown, our measurements suggest that the coupling between the qubit and the transmission line can play a key role.

F. C. W. acknowledges support from the Joint Quantum Institute and the Center for Nanophysics and Advanced Materials. The authors acknowledge discussions with Daniel Braun, David Schuster, and Andrew Houck.

[1] P. K. Day, H. G. LeDuc, B. A. Mazin, A. Vayonakis, and J. Zmuidzinas, Nature (London) **425**, 817 (2003).
[2] A. Wallraff *et al.*, Nature (London) **431**, 162 (2004).
[3] J. Hertzberg *et al.*, Nature Phys. **6**, 213 (2010).
[4] A. André *et al.*, Nature Phys. **2**, 636 (2006).
[5] R. W. Simmonds *et al.*, Phys. Rev. Lett. **93**, 077003 (2004).
[6] Z. Kim *et al.*, Phys. Rev. B **78**, 144506 (2008).
[7] J. M. Martinis *et al.*, Phys. Rev. Lett. **95**, 210503 (2005).
[8] B. S. Palmer *et al.*, Phys. Rev. B **76**, 054501 (2007).
[9] A. A. Houck *et al.*, Phys. Rev. Lett. **101**, 080502 (2008).
[10] Alexandre Blais, Ren-Shou Huang, Andreas Wallraff, S. M. Girvin, and R. J. Schoelkopf, Phys. Rev. A **69**, 062320 (2004).
[11] A. Wallraff *et al.*, Phys. Rev. Lett. **95**, 060501 (2005).
[12] T. A. Fulton and G. J. Dolan, Phys. Rev. Lett. **59**, 109 (1987).
[13] R. J. Schoelkopf *et al.*, in *Quantum Noise in Mesoscopic Physics*, edited by Y. V. Nazarov (Kluwer Academic, Dordrecht, 2003), p. 175.
[14] O. Astafiev, Y. A. Pashkin, Y. Nakamura, T. Yamamoto, and J. S. Tsai, Phys. Rev. Lett. **93**, 267007 (2004).
[15] The spectral density of noise of operator $\hat{Q}$ is defined as $S_Q(f) = \int_{-\infty}^{\infty} e^{i2\pi f\tau}\langle\hat{Q}(\tau)\hat{Q}(0)\rangle d\tau$.
[16] D. Vion *et al.*, Science **296**, 886 (2002).
[17] G. Zimmerli, T. M. Eiles, R. L. Kautz, and J. M. Martinis, Appl. Phys. Lett. **61**, 237 (1992).
[18] M. Kenyon, C. J. Lobb, and F. C. Wellstood, J. Appl. Phys. **88**, 6536 (2000).
[19] V. A. Krupenin *et al.*, J. Appl. Phys. **84**, 3212 (1998).